The effect of size ratio on the binary glass transition

Raoul A.M. Frijns, Ruben Higler and Joris Sprakel

March 14, 2016

1 Abstract

Colloidal glasses are often made by using size polydispersity or a binary mixture of sizes, though the effects of these size disparities on the colloidal glass transition are not yet completely understood. We use contrast variation multispeckle diffusing wave spectroscopy to analyse the effect of size ratio on particle dynamics near the binary glass transition. We find that both for long and short time relaxation the dynamics of the small particles either complete decouple from the large ones, moving freely through a glassy matrix, or are identical to the dynamics of the larger particles. For a size ratio of 0.35, we find a single glass transition for both particle populations and do not observe a predicted double glass transition.

2 Introduction

The changes in the dynamics of supercooled liquids approaching the glass transition has been one of the most researched, yet least understood phenomena. Whereas the liquid-crystal transition gives rise to clear changes in both structure and shear modulus; the liquid-glass transition is characterised by changes in shear modulus and a lack of any major structural changes. Binary glasses, consisting of two particle populations which differ in size, in particular have gained much attention over the last decade because of their application in bulk metallic glasses (BMGs). New types of binary BMGs have garnered attention from a material science point of view because of their high tensile strength, corrosion resistance, good processing ability paired with densities lower than their crystallised counterparts. [6] [27]

Mode coupling theory (MCT) has been used to predict dynamical behaviour of colloids approaching the glass transition, though it deviates from experiment close to the transition point. [3] [4] [16] The study of colloidal glasses is hindered by the fact that samples consisting of purely monodisperse particles will

crystalize within experimental timescales. This problem is generally circumvented either by increasing the size polydispersity of the particles [4] [8] [7] or by mixing two distinct particle populations of different sizes. [23] The effect of this non-monodispersity in size on the particle behaviour near the colloidal glass transition has been glossed over for a long time. [4] [7]

Simulations on the effects of polydsipersity [29] and binary mixtures [26] have been performed in recent years. In these simulations a decoupling of the dynamics of the smallest and largest particles of polydisperse hard spheres was observed and it was argued that polydispersity might cause the glass transition to be smeared out; the large particles arresting at lower packing fractions than the smaller ones. Simulations for a binary mixture of long range repulsive colloids have shown that the dynamics of the small particles either completely decouple or show a precursor of a double glass transition where the small particles arrest at higher packing fraction. [26] The effect of the size ratio between the particle populations in binary mixtures on the glass transition and this double transition scenario has not yet been resolved so far.

Unravelling this effect would be of great significance as it provides us with insight into the formation of binary BMGs and helps devise predictive models for the properties which specific alloys might provide. Furthermore, it will shed light on the effect of size dispersity on glassy dynamics and the process of vitrification.

One of the challenges when analysing colloidal glasses is that the particles undergo both very fast and very slow dynamics. The typical fast dynamics are caused by small movements of individual particles that do not change the structure as a whole (β-relaxation or cage rattling), while the slow dynamics are caused by larger movements where particles leave the cage that is formed by its surrounding particles (α-relaxation or 'cage breaking'). The analysis methods that are generally used are eiter either microscopy [5] [10] [22] [28] [8] or light scattering techniques. [24] [15] [7] While confocal microscopy offers the ability to visualize individual particles and allows for clear discrimination between different particle populations, generating sufficient statistics proves to be difficult. Furthermore, this technique often fails to access both fast timescales ($< 10-3$ s) due to image capturing speed limitations and long timescales ($\geq 10^2$ s) due to the enormous amounts of data generated. This hinders the ability of this technique to adequately capture both the fast β- and slow α-relaxation. Light scattering techniques like diffusing wave spectroscopy (DWS) do not suffer from poor statistics as the light samples many particles as it traverses the suspension. [25] A downside of light scattering techniques is that the distinction between different particle populations is lost, a distinction that is essential when analysing binary mixtures.

We solve this problem of light scattering by using contrast variation. By using poly(N-isopropylacrylamide) (PNIPAM) microgels with an refractive index

2

that is very close to that of the aqueous medium ($n_w = 1.330$ [17]) while the other set of particles are highly scattering polystyrene (PS) particles ($n_{PS} = 1.6$ [11]) we ensure that the scattered light only 'sees' one particle population. Applying the dual detection technique of multispeckle diffusing wave spectroscopy (MSDWS) allows us to analyse concentrated, highly scattering samples [15] and reach over seven decades of detection timescales [9] [19], enough to visualize both the α and β decays of these glassy samples.

By varying the only the size of low concentration PS tracers in a microgel matrix we investigate both the short and long time dynamics for the glass transition of binary mixtures for different size ratios $SR = \frac{r_{PS}}{r_{microgel}}$. We find that the dynamics of binary glasses follow one of two types of behaviours: for small size ratio ($SR = 0.20$) the dynamics of the small particles are completely decoupled from the larger microgel matrix both for short and long timescales, showing only hindered difusion, while intermediate to large sized tracers of $SR = 0.37$ and $SR = 1.44$ show identical dynamics to the microgel matrix. No double transition is observed where separate particle populations experience the glass transition at different packing fractions.

3   Materials and Methods

3.1   Particle system

We prepare Poly(N-isopropylacrylamide) (PNIPAM) particles with a radius of 0.9 μm according to. [13] The microgels are suspended in a 1 mM NaOH solution in order to swell them and drastically decrease their size dependence on temperature. Next, we concentrate the microgels by centrifuging at 25000 g for 5 hours. Two sets of polystyrene (PS) particles with respective radii a = 0.18 and 0.33 μm are made using emulsion polymerisation [2] and a set with a raidus of 1.3 μm is prepared using dispersion polymerisation. [14] We wash the PS particles by repeated centrifugation and resuspension steps in a 1 mM NaOH solution. Three separate mixtures of the microgels and each of the PS populations are prepared to gain a final PS volume fraction of $\phi = 0.01$ and and a high microgel packing fraction $\zeta > 1$. Dilution ranges for the microgels are prepared while keeping the PS volume fraction constant.

3.2   Multispecle Diffusing Wave Spectroscopy

3.2.1   Experimental Setup

As the dynamics of glasses involves of both fast β-relaxation, cage rattling, and slow α-relaxation, cage breaking, a measurement setup is needed that can probe a wide range of time scales. We therefore use the MSDWS setup shown in Figure 1, employing dual detection. This setup allows us to probe both short timescales using a photomultiplier tube (PMT) detector and long timescales

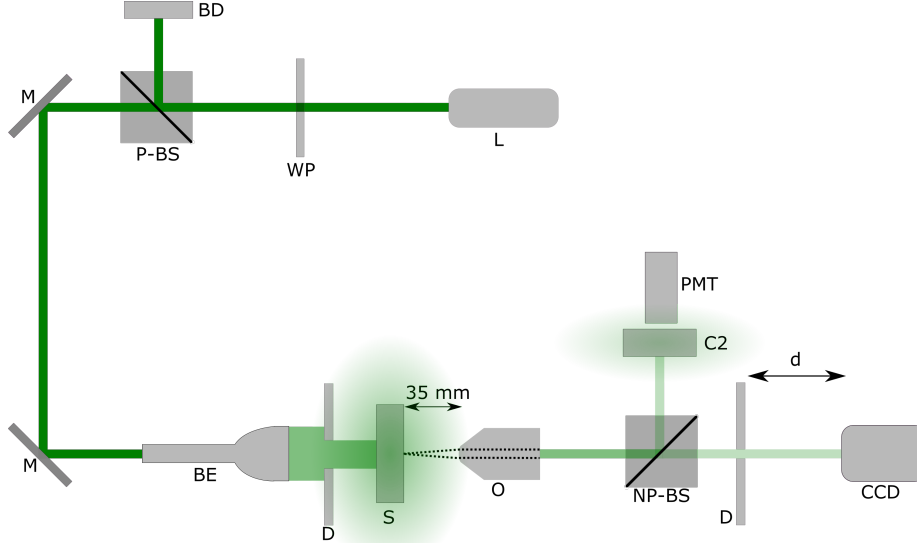using a charged coupled device (CCD) camera. [25]

Figure 1: The dual cell MSDWS experimental setup consisting of a laser (L), a wave plate (WP), a polarizing beam splitter (P-BS), a beam dump (BD), two mirrors (M), a beam expander (BE), two diaphragms (D), the sample of interest (S), an infinity corrected objective (O), a non-polarizing beam splitter (NP-BS), a CCD camera, a second cell reference sample and a PMT detector.

This MSDWS setup uses a Cobolt Samba^{TM} laser; a $\lambda = 532$ nm diode-pumped solid-state laser with a maximum output power of 1.5 W. We tune the effective power that is experienced by the sample by remotely rotating a $1/2$ λ wave plate. Changing the laser polarization allows us to tune the percentage of laser power that is diverted by a polarizing beam splitter cube away from the sample and into a beam dump. The remaining beam is subsequently expanded by a beam expanded to a diameter of 1.5 cm. The laser intensity drops near the edge of the expanded beam so we place a diaphragm with a diameter of 1.3 cm in front of the sample to ensure uniform exposure. A 2x Mitutoyo infinity-corrected objective, placed in such a way that the edge of the sample is located in the focal point, collimates the scattered light onto a 50-50 non-polarizing beam splitter. Half of the light passes through another diaphragm and is detected by a Fasttech^{TM} charge coupled device camera. The camera is placed a distance d behind the second diaphragm. The other half of the light intensity is projected onto a second, purely diffusive scattering sample, this is needed to ensure ergodicity of the signal. [19] [9] The secondarily scattered light is detected by a PMT detector. The entire setup is encased in anodized black steel to block stray light.

The high max output power of the laser ensures that we can analyse even highly scattering samples. In order to ensure laser stability for samples that require illumination with a much lower laser power, a $1/2$ λ wave plate and polarizing beam splitter allow us to keep the laser output consistent for all measurements at 1.3 W while tuning the percentage of laser power that reaches the sample. The camera captures 127x128 pixels sized frames at 500 fps. For every sample we determine the appropriate effective laser power that uses the dynamic range of the camera to its fullest without pixels exceeding the maximum intensity. This generally falls within the range of 270-325 mW.

PMT detection gives reliable data at very fast time scales ($\geq 10^{-3}$ ms). For long time scales the time needed to gather ample statistics increases exponentially, imposing practical limitations on measuring slow dynamics. The CCD camera can detect many speckles simultaneously, each pixel effectively acting as a separate correlator. This way the ensemble average is obtained in a single frame instead of needing to average over time.

The size of the speckles on the CCD camera is determined by

$$s = d\lambda/a \tag{1}$$

where s is the speckle size, d is the distance between the diaphragm and the CCD camera, λ is the wavelength of the laser and a is the diaphragm diameter. The speckle size should be tuned to make sure that speckles are small enough to yield as much statistics as possible but not so small that the signal for a single pixel contains the information of multiple speckles. For our experiments we set d = 15 cm and a = 2 mm, yielding a speckle size of 40 μm. The speckle size in pixels can also be determined empirically by calculating the spatial intensity autocorrelation function

$$C(p) = \frac{< I_i I_{i+p} >_i}{< I_i^2 >_i} \tag{2}$$

over all the pixels in a frame. Where I_i is the measured intensity of pixel i, I_{i+p} is the measured intensity of a pixel which is a distance p removed from pixel I_i. The speckle size is defined as the position of the first minimum in Equation 2. The calculated speckle size for the conditions used in our measurements is 6 pixels.

3.2.2 Data processing

In order to extract information from the camera images, we calculate the ensemble-averaged, temporal autocorrelation function of the measured intensities using

$$g_2(t, t_0) = \frac{< I_i(t_0) I_i(t_0 + t) >_i}{< I_i(t_0) >_i < I_i(t_0 + t) >_i} \tag{3}$$

where $I_i(t_0)$ is the intensity of a pixel at the starting time t_0. Unlike in conventional, PMT detected $g_2(t_0, t)$, we acquire the ensemble average over pixels

instead of over different t_0.

The measured autocorrelation function $g_2(t)$ can be converted into the field autocorrelation function $g_1(t)$ using the Siegert relation [20]

$$g_1(t) = \beta\sqrt{g_2(t) - 1} \tag{4}$$

where β is a setup dependent coefficient. We find that the timescale of the camera measurements is limited by slow vibrations in the setup. Temporal autocorrelation curves of a static glass frit show partial or complete decorrelation at timescales typically in the order of 10^5-10^6 ms. We therefore cut off the camera data at $3 \cdot 10^4$ ms.

PMT detection assumes that the detected signal originates from an ergodic source. The two-cell technique allows us to measure nonergodic samples such as glasses. [19] [9] If light is scattered by a nonergodic and an ergodic sample sequentially the overall signal will be ergodic. The measured correlation function $g_2^M(t) - 1$ is a the product of the correlation functions of the sample of interest $g_2^S(t) - 1$ and a reference sample in the second cell $g_2^R(t) - 1$.

$$g_2^M(t) - 1 = \left(g_2^S(t) - 1\right)\left(g_2^R(t) - 1\right) \tag{5}$$

However, this means that as soon as the correlation of the reference sample has decayed to zero, no more data on the sample of interest can be acquired. It is therefore of importance that the reference sample decays slowly. We use a $\phi = 0.01$ suspension of PS with a radius of 1 μm in glycerol in a cell thickness of 2 mm. This sample decorrelates in the time frame of 40-100 ms so we cut off our PMT data at 30 ms. Combined with the frame rate of the camera of 500 fps this gives us a region of 2-30 ms where the techniques overlap. This overlap is used to determine the β value from the Siegert relation for the camera detection. This β varies between samples, in part because the effective laser intensity is varied between samples. For every sample a β value was found that gave excellent agreement between the camera and PMT data in the overlap.

Combining different detection techniques allows us to measure correlations reliably on timescales ranging from 10^{-3} to 10^4 ms.

4   Results and Discussion

Through contrast variation we can follow the dynamics of a single population of particles exclusively. As swollen PNIPAM microgels contain >95% water, their refractive index matches that of the aquous medium ($n_w = 1.33$) very well, whereas the PS particles show a clear index mismatch ($n_{PS} = 1.6$). This allows us to measure how the dynamics of the PS tracers of different sizes are effected microgel matrix approaching the glass transition. We first examine the dynamics of both the limits of large (1.44) and small (0.20) size ratios in order to obtain references for both strongly coupled dynamics for large tracers

and completely decoupled dynamics small tracers. Next we investigate how this compare to the dynamics of at intermediate size ratio of 0.37.

In order to determine the dynamics of the microgel matrix, we first measure the decorrelation function $g_2(t) - 1$ of a binary mixture of microgel matrix and PS with $SR = 1.44$, for a wide range of microgel packing fractions ζ. For $\zeta \geq 0.76$ the $g_2(t) - 1$ shows a partial decay on short timescales to a plateau value followed by a full decay from the plateau value to zero on long timescales. As ζ is lowered the plateau value decreases as do the decays for both long and short timescales. For $\zeta < 0.76$ the plateau and second decay disappear altogether and the correlation curve reduces to a single, full decay.

We fit $g_2(t) - 1$ to either

$$g_2(t) - 1 = e^{\frac{t}{\tau_2*}^\gamma} \tag{6}$$

if it shows full decorrelation in a single decay, or

$$g_2(t) - 1 = d e^{(\frac{t}{\tau_1*})^{\gamma_1}} - (1-d) e^{(\frac{t}{\tau_2*})^{\gamma_2}} \tag{7}$$

if it shows a two-step decay separated by a plateau. Here $(1-d)$ is the plateau height for $\tau_1* < \tau_2*$ and the γ are stretch exponentials. We expect sub-diffusive, $\gamma < 1$, behaviour for our more concentrated samples, as diffusion of the PS particles is inherently hindered by the matrix.

τ_1* and τ_1* are the characteristic decay times of the autocorrelation functions in equations 6 and 7. Unlike other scattering techniques like dynamic light scattering, the measured characteristic decay time does not equal that of the sample. Because the light is scattered many times before being detected, the measured decay time depends both on the sample thickness L and the mean free path $l*$ of the photons, which is the length over which the direction of the light is randomized. These parameters are related through $\tau* = (\frac{l*}{L})^2 \tau$ [15], where τ is the delay time of the particles.

In order to determine $l*$ for every sample S, we relate it to a reference sample R with a known $l*$ through

$$\frac{l_S*}{I_S} = \frac{l_R*}{I_R} \tag{8}$$

where I is the transmittance intensity. Equation 8 only applies if effective laser power and L are kept constant. l_R* is determined by fitting the $g_1(t)$ for four measurements with different values of L to equation 16.39b of reference [15].

The occurrence of a double decay is to be expected for supercooled liquid and glassy samples because of their short time cage rattling dynamics (β-decay) and long time cage breaking dynamics (α-decay). For liquid samples we would expect only a single decay as the particles move more freely and every movement

7

is essentially cage breaking. Therefore when analysing the liquid-glass transition we are interested mainly in the cage breaking dynamics. Figure 2 (red triangles) shows the ζ dependence of $\frac{\tau}{\tau_0}$, where τ_0 is the decay time for the PS particles in the diluted limit.
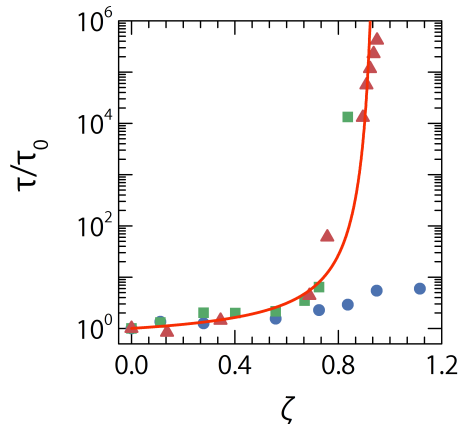

Figure 2: Relative relaxation times $\frac{\tau}{\tau_0}$ for polystyrene particles at constant $\phi_{PS} = 0.01$ in a matrix of PNIPAM microgels versus the packing fraction ζ of the microgels for PS:PNIPAM size ratios of 1.44 (triangles), 0.33 (squares) and 0.20 (circles). A Vogel-Fulcher-Tammann fit (Equation 9) of the data for the 1.44 size ratio is shown (solid line) for the parameters $A = 0.7$ and $\zeta_0 = 0.97$.

For a size ratio of 1.44, this dependence is described very well by the Vogel-Fulcher-Tammann (VFT) equation

$$\frac{\tau}{\tau_0} = e^{\frac{A\zeta}{\zeta_0 - \zeta}} \tag{9}$$

Equation 9 is an empirical function that holds for both the molecular [1] [12] and colloidal [4] glass transitions. For our fit we find $A = 0.7$ and $\zeta_0 = 0.97$. We define that the glass transition occurs at ζ_g where $\frac{\tau_{\zeta_g}}{\tau_0} = 10^6$, resulting in $\zeta_g = 0.92$.

Though we observe that the PS particles experience a glass transition they cannot form a glass by themselves as ϕ_{PS} is far too low. As $SR > 1$ the PS particles will only arrest if the microgel matrix does. Although the system is binary, the dynamics we observe are shared by both particle populations. We have therefore indirectly determined the dynamics of the microgels approaching glass transition. This gives us a good reference to compare the dynamics of other size ratios. The dynamics of the microgels are not be significantly influenced by the size ratio as the number of PS tracers is very small compared to the microgels.

Next we repeat the experiments and analysis for $SR = 0.20$. Even at $\zeta > 1$, the correlation function $g_2(t) - 1$ decays fully in a single, fast decay and $\frac{\tau}{\tau_0}$ varies only a single decade with increasing ζ (blue circles in Figure 2). Even though the microgels will still form a glass at $\zeta = 0.92$, the small PS particles do not experience a glass transition at all and are barely hindered by the microgel glass. The two particle populations are completely decoupled.

When considering the geometry of small spheres moving through a matrix of larger spheres, this decoupling makes perfect sense. When considering the most closely packed system of spheres, the smallest openings can be compared to three touching circles. A sphere of with a size ratio of 0.15 compared to the larger ones will still be able to move through these openings. As our glasses are made up of randomly packed spheres, rather than closely packed, the openings will on average be bigger. It is therefore plausible that at a size ratio of 0.20 the small particles can move almost diffusively inside a disordered matrix of the large particle population.

The interesting regime is at intermediate size ratios where the particles are significantly smaller than the large particles but large enough as to not diffuse freely through a random close packed matrix of the large particles. Simulations have predicted a double transition in this regime, where the small particles arrest at higher ζ than the large ones. We evaluate this regime using $SR = 0.20$ and observe that the correlation curves resemble those at $SR = 1.44$; a single, full decay at low concentrations and a plateau separated double decay at high concentrations. When we consider the dependence of $\frac{\tau}{\tau_0}$ on ζ (green squares in Figure 2) we notice that it overlaps within experimental margins with the VFT fit for the $SR = 1.44$ scenario. This indicates that is no difference in the long time dynamics between binary mixtures of size ratios 1.44 and 0.37.

This finding, a single glass transition at a size ratio of 0.37 contradicts earlier simulations [26]. There, a clear decoupling of the motions of the small and large particles was found for a size ratio of 0.35. This disparity between simulation and experiment can be explained by the simulated repulsive interactions and the volume regulation of the microgels. The PNIPAM microgels do not display the long range repulsion that was simulated by Voigtmann and Horbach. Furthermore, we have previously proposed a model for soft colloidal glasses which considers the osmotic shrinkage of microgels at high ζ. As the PS tracer particles do not display this osmotic shrinkage, the effective volume ratio that is experienced by the tracer particles will be higher than the 0.37 at low ζ. This size regulation effect was not considered in the simulation in REF x. It is interesting to note that while both type of particles are generally considered 'soft', they display very different behaviours at this size ratio.

So far, we have only looked at the particle dynamics at long timescales. However, recent publications have argued that when considering liquid dynamics, both long time (diffusional) and and short time (vibrational) motions are

important. [21] We can extract the short time dynamics of our system from our correlation curves as well by converting $g_2(t) - 1$ to $g_1(t)$ using the Siegert relation in Equation 4. The mean squared displacement (MSD) $< \Delta r^2 >$ of our tracer particles can be determined from $g_1(t)$ by performing a numerical inversion of equation 4 from reference [18], provided $g_1(t)$ has not yet fully decayed.
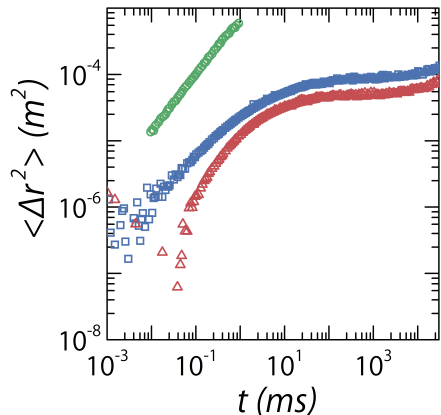

Figure 3: The mean square displacement $< \Delta r^2 >$ of Polystyrene tracers inside a PNIPAM microgel matrix for PS:PNIPAM size ratios of 1.44 (triangles), 0.33 (squares) and 0.20 (circles) near the microgel glass transition ($\zeta = 0.84$ for size ratios 0.33 and 0.2 and $\zeta = 0.85$ for size ratio 1.44).

The $< \Delta r^2 >$ of the systems with size ratios of 1.44 and 0.33 show very similar behaviour near the microgel glass transition ($\zeta = 0.95$), exhibiting a caging plateau at approximately the same height, whereas the system with a size ratio of 0.20 does not show a caging plateau at all. This behaviour, shown in Figure 3, indicates that the small particles for $SR = 0.20$ do not feel the matrix at all on short timescales.

The caging plateaus in the MSD give us the localisation lenghts δ of the PS particles by taking the square root of the value of $< \Delta r^2 >$ at the plateau. For $SR = 1.44$ and $SR = 0.33$ the δ are equal within experimental margins for all measured ζ as is shown in Figure 4. This shows that while there is a clear bifurcation of the short time dynamics in glasses with a size ratio of 0.20, glasses with size ratios of 0.33 and 1.44 only show a single dynamical population.

5   Conclusions

We have found that there are two regimes for particle dynamics in binary colloidal suspensions approaching the glass transition. For a very large size dis-
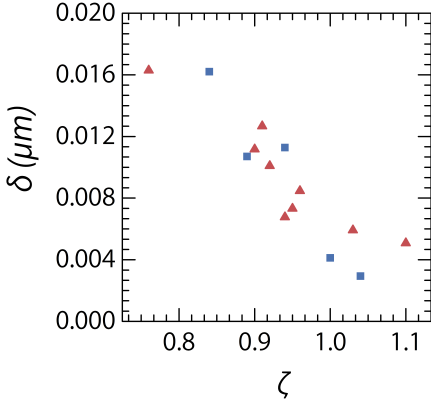
Figure 4: The localisation length of PS particles in a microgels with size ratios of 1.44 (circles), 0.33 (squares) show identical behaviour. No localisation lengths could be determined for the particle system with a size ratio of 0.20 as the there is no caging plateau in the MSD.

parity between the small and large particles there is a complete decoupling of the dynamics of the small and large particles, where the small particles are able to diffuse freely through a glass of the large particles. For both intermediate and large size ratios the particle dynamics of the small and large particles are indistinguishable, experiencing both similar α-relaxation times as well as caging lenghts. These two regimes are separated by a sharp transition as no intermediate double transition behaviour was found.

In order to come to a general understanding of the binary glass transition it is necessary to investigate the effect of other factors that govern particle dynamics. The inclusion of a long range repulsive potential has shown to able to be the difference between a coupled and decoupled glass at the same size ratio. Different types of interaction potentials should be analysed in future work to elucidate their effect on the binary glass transition.

References

[1] C A Angell. Structural instability and relaxation in liquid and glassy phases near the fragile liquid limit. *Journal of Non-Crystalline Solids*, 102(13):205–221, 1988.

[2] Jeroen Appel, Niek de Lange, Hanne M van der Kooij, Ties van de Laar, Jan Bart ten Hove, Thomas E Kodger, and Joris Sprakel. Temperature Controlled Sequential Gelation in Composite Microgel Suspensions. *Particle & Particle Systems Characterization*, 32(7):764–770, 2015.

[3] B. Bernu, J. P. Hansen, Y. Hiwatari, and G. Pastore. Soft-sphere model for the glass transition in binary alloys: Pair structure and self-diffusion. *Physical Review A*, 36(10):4891–4903, 1987.

[4] G. Brambilla, D. El Masri, M. Pierno, L. Berthier, L. Cipelletti, G. Petekidis, and A. B. Schofield. Probing the equilibrium dynamics of colloidal hard spheres above the mode-coupling glass transition. *Physical Review Letters*, 102(8):1–4, 2009.

[5] A. D. Dinsmore, Eric R. Weeks, Vikram Prasad, Andrew C. Levitt, and D. A. Weitz. Three-dimensional confocal microscopy of colloids. *Applied optics*, 40(24):4152–9, 2001.

[6] Gang Duan, Donghua Xu, Qing Zhang, Guoyun Zhang, Tahir Cagin, William L. Johnson, and William A. Goddard. Molecular dynamics study of the binary Cu46Zr54 metallic glass motivated by experiments: Glass formation and atomic-level structure. *Physical Review B - Condensed Matter and Materials Physics*, 71(22):1–9, 2005.

[7] Markus Franke, Sebastian Golde, and Hans Joachim Schöpe. Solidification of a colloidal hard sphere like model system approaching and crossing the glass transition. *Soft matter*, 10(29):5380–9, 2014.

[8] Antina Ghosh, Vijayakumar Chikkadi, Peter Schall, and Daniel Bonn. Connecting Structural Relaxation with the Low Frequency Modes in a Hard-Sphere Colloidal Glass. *Phys. Rev. Lett.*, 107(18):188303, oct 2011.

[9] J. L. Harden and V. Viasnoff. Recent advances in DWS-based microrheology. *Current Opinion in Colloid and Interface Science*, 6(5-6):438–445, 2001.

[10] J Hendricks, R Capellmann, a B Schofield, S U Egelhaaf, and M Laurati. Different mechanisms for dynamical arrest in largely asymmetric binary mixtures. *Physical review. E, Statistical, nonlinear, and soft matter physics*, 91(3):032308, 2015.

[11] Xiaoyan Ma, Jun Q Lu, R Scott Brock, Kenneth M Jacobs, Ping Yang, and Xin-Hua Hu. Determination of complex refractive index of polystyrene microspheres from 370 to 1610 nm. *Physics in Medicine and Biology*, 48(24):4165, 2003.

[12] L.-M. Martinez and C A Angell. A thermodynamic connection to the fragility of glass-forming liquids. *Nature*, 410(6829):663–667, apr 2001.

[13] Zhiyong Meng, Michael H Smith, and L Andrew Lyon. Temperature-programmed synthesis of micron-sized multi-responsive microgels. *Colloid and Polymer Science*, 287(3):277–285, 2009.

[14] Anthony James Paine, Wayne Luymes, and James McNulty. Dispersion polymerization of styrene in polar solvents. 6. Influence of reaction parameters on particle size and molecular weight in poly(N-vinylpyrrolidone)-stabilized reactions. *Macromolecules*, 23(12):3104–3109, 1990.

[15] D. J. Pine, D. A. Weitz, P. M. Chaikin, and E. Herbolzheimer. Diffusing wave spectroscopy. *Physical Review Letters*, 60(12):1134–1137, 1988.

[16] David R Reichman and Patrick Charbonneau. Mode-coupling theory. *Journal of Statistical Mechanics: Theory and Experiment*, 2005(05):P05013, 2005.

[17] M. Reufer, P. D??az-Leyva, I. Lynch, and F. Scheffold. Temperature-sensitive poly(N-Isopropyl-Acrylamide) microgel particles: A light scattering study. *European Physical Journal E*, 28(2):165–171, 2009.

[18] E Sarmiento-Gomez. A dynamical light scattering technique and its application in viscoelastic networks in soft matter. *... for Optics (ICO ...*, 8011:1–9, 2011.

[19] F Scheffold, S E Skipetrov, S Romer, and P Schurtenberger. Diffusing-wave spectroscopy of nonergodic media. *Physical review. E, Statistical, nonlinear, and soft matter physics*, 63(6 Pt 1):061404, 2001.

[20] A J F Siegert. *On the fluctuations in signals returned by many independently moving scatterers*. Radiation Laboratory, Massachusetts Institute of Technology, 1943.

[21] K Trachenko and V V Brazhkin. Duality of liquids. *Scientific reports*, 3:2188, 2013.

[22] A. van Blaaderen and P. Wiltzius. Real-Space Structure of Colloidal Hard-Sphere Glasses. *Science*, 270(19):1177–1179, 1995.

[23] Frank van Swol and Dimiter N. Petsev. Molecular dynamics simulation of binary hard sphere colloids near the glass transition. *RSC Advances*, 4(41):21631, 2014.

[24] Virgile Viasnoff and Fran\cois Lequeux. Rejuvenation and Overaging in a Colloidal Glass under Shear. *Phys. Rev. Lett.*, 89:65701, 2002.

[25] Virgile Viasnoff, François Lequeux, and D. J. Pine. Multispeckle diffusing-wave spectroscopy: A tool to study slow relaxation and time-dependent dynamics. *Review of Scientific Instruments*, 73(6):2336, 2002.

[26] Th Voigtmann and J. Horbach. Double transition scenario for anomalous diffusion in Glass-Forming mixtures. *Physical Review Letters*, 103(20):8–11, 2009.

[27] W. H. Wang, C. Dong, and C. H. Shek. Bulk metallic glasses. *Materials Science and Engineering R: Reports*, 44(2-3):45–90, 2004.

[28] E. R. Weeks. Three-Dimensional Direct Imaging of Structural Relaxation Near the Colloidal Glass Transition. *Science*, 287(5453):627–631, 2000.

[29] Emanuela Zaccarelli, Siobhan M Liddle, and Wilson C K Poon. On polydispersity and the hard sphere glass transition. *Soft matter*, 11(2):324–30, 2015.